Study of Electromagnetic Multipole Transition Half-Lives of One-Hole ^{15}O – ^{15}N and One-Particle ^{17}O – ^{17}F Mirror Nuclei

Mohammadreza Pahlavani and Behnam Firoozi

Department of Nuclear Physics, Faculty of Science, University of Mazandaran, P.O. Box 47415-416, Babolsar, Iran

Reprint requests to M. P.; E-mail: m.pahlavani@umz.ac.ir

Z. Naturforsch. **68a,** 709 – 714 (2013) / DOI: 10.5560/ZNA.2013-0056
Received December 25, 2012 / revised July 29, 2013 / published online October 2, 2013

Energy spectrum and wave functions are obtained numerically with a potential consisting of Woods–Saxon, Coulomb, and spin–orbit coupling parts for the nuclei ^{15}O, ^{15}N, ^{17}O, and ^{17}F. The radial parts of the wave functions are used to calculate some matrix elements of electromagnetic transitions. These results are applied to calculate half-lives of low-lying exited states in the one-particle ^{17}O and ^{17}F as well as in the one-hole ^{15}O and ^{15}N isotopes. The calculated half-lives are compared with available experimental and theoretical results based on harmonic oscillator wave functions and Weisskopf units. In comparison with the results calculated from the other methods, our results based on the Woods–Saxon potential indicate a satisfactory agreement with accessible experimental data.

Key words: Multipole Moments; Woods–Saxon Potential; One-Particle Nuclei; One-Hole Nuclei; Electromagnetic Transition Probability.
PACS numbers: 21.10.kx; 21.60.cs; 23.20.$^{-}$g

1. Introduction

The A-nucleon Schrödinger equation by the Hamiltonian with complete nuclear potential cannot be solved analytically. Therefore, one has to look for reasonable approximation methods to solve this many-body problem of strongly interacting particles system. An elegant approximation which is widely used for such a system is the mean field approximation [1]. The mean-field theory represents the average interaction of one nucleon with the other nucleons of a nuclear complex system. Moreover, this theory with phenomenological single-particle potential is a powerful tool to describe low-energy nuclear phenomena. There are several potentials that can be a candidate for treating nuclear structures, of which the most frequently-used is the three-dimensional harmonic oscillator potential (HO). The single-particle Schrödinger equation with three-dimensional harmonic oscillator potential has been solved exactly in literature [2, 3].

Among other existing phenomenological potentials in literature, the realistic single-particle Woods–Saxon (W–S) potential [4 – 6] is reasonable to describe many properties of nuclei such as the nuclear equilibrium deformations and moments, the mean square radii, the nucleon binding energies, the structure of the high-spin isomers, the fission barriers, and some other properties of the single-particle effects for strongly deformed and fast-rotating nuclei [7]. A complete set which consists of Woods–Saxon , Coulomb, and spin–orbit coupling, gives a complete Hamiltonian that reproduces the experimentally observed single-particle energies in the mean-field theory. An exact solution of the Schrödinger equation for the central Woods–Saxon potentials received much interest in recent years. Therefore, many efforts have been made to solve it [8, 9]. The wave equations with the Woods–Saxon potential can be solved analytically only for s-waves due to the centrifugal potential barrier using different methods [10, 11].

The eigenfunctions and eigenvalues of the Schrödinger equation with mean-field phenomenological potentials can be used to describe various electromagnetic observables which are related to electromagnetic transitions [1, 12]. The electromagnetic radiation field can be expanded as a series of multipoles containing spherical harmonic oscillators. The field is also quantized in terms of photons. Creation and annihilation of photons are described in the occupation number representation [3]. The electromagnetic processes are excellent tests for the validity of various assumptions underlying the shell structure of the nuclei [2]. In particular,

the decay properties produced by the solutions of the Schrödinger equation are appropriate indicators for the degree of validity of the mean-field potential. The transition from the initial to the final state has been mediated by one of the multipole terms in the expansion of the radiation field [12].

In this investigation, at first in the second section, we discuss the nuclear mean field using a complete set of potentials to obtain the eigenvalues and eigenfunctions of the single-particle Schrödinger equation for the typical one-particle $^{17}\mathrm{O}-^{17}\mathrm{F}$ and one-hole $^{15}\mathrm{O}-^{15}\mathrm{N}$ mirror nuclei. In the third section, various theoretical numerically calculated results of the electromagnetic transition properties for the aforementioned nuclei are presented and compared with the accessible experimental data. Finally, a brief conclusion is provided in the last section.

2. Solutions of the Radial Schrödinger Equation for the Nuclear Potential

In the mean-field approximation, each nucleon can be viewed as moving in an external field created by the remaining $A-1$ nucleons. The nuclear mean-field Hamiltonian is defined by the equation

$$H_{\mathrm{MF}} = T + V_{\mathrm{MF}}\,, \tag{1}$$

which is supposed and treated as an A-nucleon system. The remaining problem is how to determine the reasonable mean-field potential. In our example, the generated mean-field potential is central, i. e. only a function of r. Two practical and phenomenological potentials widely used as mean field are [13, 14]

$$V_{\mathrm{MF}} = \begin{cases} V_{\mathrm{HO}}(r) = -V_1 + \frac{1}{2} m_{\mathrm{N}} \omega^2 r^2\,, \\ V_{\mathrm{WS}}(r) = \frac{-V_0}{1+\exp\left(\frac{r-R}{a}\right)}\,, \end{cases} \tag{2}$$

with R, a, V_0, V_1, and ω as nuclear radius, surface diffuseness, depth of nuclear well, and angular frequency, respectively. These parameters are evaluated by fitting with exact experimental data [7, 14]:

$$\begin{aligned} &R = r_0 A^{\frac{1}{3}} = 1.27 A^{\frac{1}{3}}\,\mathrm{fm}\,,\quad a = 0.67\,\mathrm{fm}\,,\\ &V_0 = \left(51 \pm 33\frac{N-Z}{A}\right)\mathrm{MeV}\,,\\ &V_1 = 48.6\,\mathrm{MeV}\,,\quad \hbar\omega = \left(45A^{-\frac{1}{3}} - 25A^{-\frac{2}{3}}\right)\mathrm{MeV}\,, \end{aligned} \tag{3}$$

where the $+$ and $-$ signs are adopted for protons and neutrons, respectively. The nuclear Hamiltonian for the presented complete set of potentials is [3, 7] therefore

$$\begin{aligned} H = &-\frac{\hbar^2}{2m_{\mathrm{N}}}\left[\nabla_r^2 - \frac{L^2}{\hbar^2 r^2}\right] + V_{\mathrm{WS}}(r)\\ &+ V_{\mathrm{C}}(r) + V_{\mathrm{LS}}(r) L\cdot S\,, \end{aligned} \tag{4}$$

where $V_{\mathrm{C}}(r)$ and $V_{\mathrm{LS}}(r)$ are central coulomb and spin–orbit coupling potentials, respectively. These potentials are presented as following [1, 7]:

$$V_{\mathrm{C}}(r) = \frac{Z\mathrm{e}^2}{4\pi\varepsilon_0} \begin{cases} \frac{3-\left(\frac{r}{R}\right)^2}{2R} & r \le R\,, \\ \frac{1}{r} & r > R\,, \end{cases} \tag{5}$$

$$V_{\mathrm{LS}}(r) = \upsilon_{\mathrm{LS}}^{(0)} \left(\frac{r_0}{\hbar}\right)^2 \frac{1}{r}\left[\frac{\mathrm{d}}{\mathrm{d}r} V_{\mathrm{WS}}(r)\right], \tag{6}$$

where $\upsilon_{\mathrm{LS}}^{(0)} = -0.44$ is the strength of the spin–orbit coupling interaction. Washing out the angular dependence, the radial part of the Schrödinger equation for wave function $\phi(r)$ is

$$\begin{aligned} &\left\{ -\frac{\hbar^2}{2m_{\mathrm{N}}}\left[\nabla_r^2 - \frac{l(l+1)}{r^2}\right] + V_{\mathrm{WS}}(r) \right.\\ &+ V_{\mathrm{C}}(r) + \frac{1}{2}\left[j(j+1) - l(l+1) - \frac{3}{4}\right]\\ &\left.\cdot \hbar^2 V_{\mathrm{LS}}(r)\right\} \phi_{nlj}(r) = \varepsilon_{nlj}\phi_{nlj}(r)\,. \end{aligned} \tag{7}$$

The notations $\phi_{nlj}(r)$ and ε_{nlj} indicate the radial wave function and energy spectrum, the parameters n, l, and j are energy level quantum, orbital, and total angular momentum quantum numbers, respectively. This second-order radial differential equation is solved numerically via Francis [15] by the QR (Q and R stand for orthogonal matrix and upper triangular matrix, respectively) factorization algorithm [16] to obtain the energy spectrum and the corresponding wave functions. r is considered between 0.01 and 10 fm to eliminate singularity and by the use of $\mathrm{d}r = 0.01$ steps to construct a 1000×1000 matrix of the Hamiltonian. Two constraints are imposed on this solution:

$$\lim_{r\to\infty} \phi_{nlj}(r) = 0\,, \tag{8}$$

$$\int_0^\infty \left|\phi_{nlj}(r)\right|^2 r^2\,\mathrm{d}r = 1\,. \tag{9}$$

One-particle and one-hole nuclei consist of one particle outside of an inner core or one hole in a completely filled valance space with its Fermi level at some magic number [2]. These nuclei are always odd-mass or odd-A nuclei, or simply odd nuclei. According to their proton number Z and neutron number N, they are called even–odd or odd–even nuclei. Finally, the

calculated values of the one-particle and one-hole energy states ε_{nlj} of ^{15}O, ^{15}N, ^{17}O, and ^{17}F mirror nuclei are presented in Table 1, and the energy difference between low-lying excited states and ground state are shown in Table 2. The eigenfunctions $\phi_{nlj}(r)$ for the Fermi and first excited states of these typical mirror nuclei are shown in Figures 1 and 2.

3. Calculation of Electromagnetic Transition Half-Lives

Consider an electromagnetic transition evolving a low-lying excited nucleus to its ground state. The transition from the initial (i) to the final (f) state can be expanded as multi-pole terms obeying quantum mechanical conservation rules on spin and parity [18]. The time-dependent perturbation theory is applied to calculate the transition probability. Starting point in this type of calculation is [3]

$$T_{\mathrm{fi}}^{(\sigma\lambda)} = \frac{2(\lambda+1)}{\varepsilon_0 \hbar\lambda\left[(2\lambda+1)!!\right]^2} \cdot \left(\frac{E_\gamma}{\hbar c}\right)^{2\lambda+1} B(\sigma\lambda;\mathrm{i}\to\mathrm{f}), \tag{10}$$

Table 1. Energy spectrum of one-hole $^{15}\mathrm{O}-^{15}\mathrm{N}$ and one-particle $^{17}\mathrm{O}-^{17}\mathrm{F}$ mirror nuclei by considering Woods–Saxon, Coulomb, and spin–orbit potentials.

Single particle orbits (^nL_j)	$\varepsilon_{nlj}(^{15}\mathrm{O})$ (MeV)	$\varepsilon_{nlj}(^{15}\mathrm{N})$ (MeV)	$\varepsilon_{nlj}(^{17}\mathrm{O})$ (MeV)	$\varepsilon_{nlj}(^{17}\mathrm{F})$ (MeV)
$^1s_{1/2}$	−32.260	−28.109	−30.075	−24.954
$^1p_{3/2}$	−19.361	−15.639	−17.987	−13.396
$^1p_{1/2}$	−13.795	−10.099	−13.202	−8.633
$^1d_{5/2}$	−6.713	−3.469	−6.0853	−2.085
$^2s_{1/2}$	−4.23	−1.333	−3.823	−0.277

Table 2. Experimental and numerically computed γ-ray emitted energy (MeV) in transition between low-lying excited states and ground state of the one-hole $^{15}\mathrm{O}-^{15}\mathrm{N}$ and the one-particle $^{17}\mathrm{O}-^{17}\mathrm{F}$ mirror nuclei by considering Woods–Saxon, Coulomb, and spin–orbit potentials.

Isotope	^{15}N	^{15}O	^{17}O	^{17}F
Transition mode	$^1p_{1/2}\to{}^1p_{3/2}$	$^1p_{1/2}\to{}^1p_{3/2}$	$^2s_{1/2}\to{}^1d_{5/2}$	$^2s_{1/2}\to{}^1d_{5/2}$
Experimental [17]	6.324	6.176	0.871	0.495
Computed value	5.540	5.566	2.262	2.303

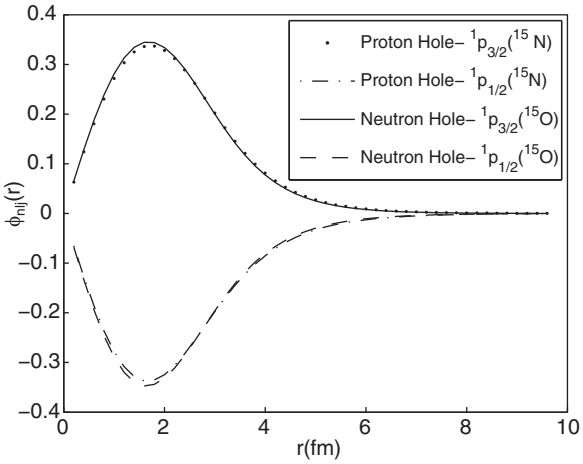

Fig. 1. Ground state and first excited state wave functions for one-hole ^{15}O and ^{15}N mirror nuclei.

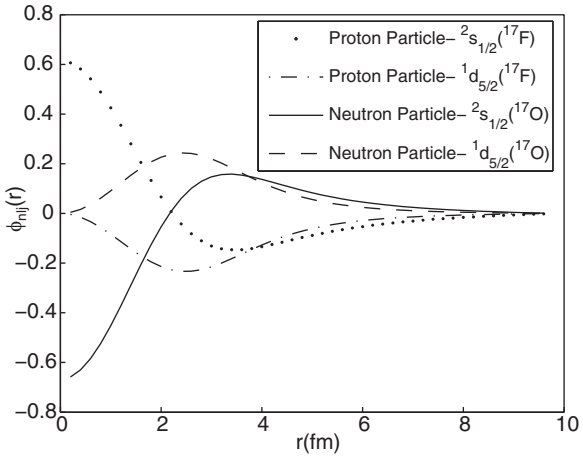

Fig. 2. Ground state and first excited state wave functions for one-particle ^{17}O and ^{17}F mirror nuclei.

where $T_{\mathrm{fi}}^{(\sigma\lambda)}$ is the transition probability for the multipole transition of order λ. The sources of transition are either of electric or magnetic type, designated by an index σ such that $\sigma = E$ or $\sigma = M$. E_γ is the energy of the emitted γ ray. Also, for both one-particle and one-hole nuclei, the reduced transition probability $B(\sigma\lambda)$ is defined as

$$B(\sigma\lambda;\mathrm{i}\to\mathrm{f}) = \frac{1}{2J_\mathrm{i}+1}\left|\langle \mathrm{f}\parallel M_{\sigma\lambda}\parallel \mathrm{i}\rangle\right|^2. \tag{11}$$

It should be noted that the one-particle states $|i\rangle$ and $|f\rangle$ are the physical single-particle states include the core, and the physical one-hole states involve the

Hartree–Fock vacuum $|\mathrm{HF}\rangle$. The single particle multipole tensor operator $M_{\sigma\lambda}$ for electric $(M_{\mathrm{E}\lambda})$ and magnetic $(M_{\mathrm{M}\lambda})$ transition in usual notation with Condon–Shortley phase convention [19] is

$$M_{\mathrm{E}\lambda} = Q_\lambda = \sum_\mu \sum_{j=1}^{A} e(j) r_j^\lambda Y_{\lambda\mu}(\Omega_j)\,, \tag{12}$$

$$M_{\mathrm{M}\lambda} = M_\lambda = \frac{\mu_\mathrm{N}}{\hbar c} \sum_\mu \sum_{j=1}^{A} \left[\frac{2}{(\lambda+1)} g_l^{(j)} l(j) + g_s^{(j)} s(j) \right] \cdot \nabla_j \left[r_j^\lambda Y_{\lambda\mu}(\Omega_j) \right], \tag{13}$$

where $e(j)$ is the electric charge, and $l(j)$ and $s(j)$ are the orbital and spin angular momentum of nucleon j, respectively. The gyromagnetic ratios are $g_s^{(j)} = g_\mathrm{p} = 5.586$ for proton and $g_s^{(j)} = g_\mathrm{n} = -3.826$ for neutron. The orbital g factors are $g_l^{(j)} = 1$ for protons and $g_l^{(j)} = 0$ for neutrons [3]. The transition probability is decreased drastically by increasing the multi-polarity. Therefore the most probable transition is the lowest allowed multi-polarity by the angular momentum and parity selection rules [4]. For a λ-pole transition between nuclear states of angular momenta J_i and J_f, the angular momentum selection rule is $|J_\mathrm{f} - J_\mathrm{i}| \le \lambda \le |J_\mathrm{f} + J_\mathrm{i}|$, and the parity selection rule is [2]

$$\pi_\mathrm{i}\pi_\mathrm{f} = \begin{cases} (-1)^\lambda & \text{for } \mathrm{E}\lambda \\ (-1)^{\lambda-1} & \text{for } \mathrm{M}\lambda\,. \end{cases} \tag{14}$$

From the Wigner–Eckart theorem which is introduced by Wigner [20] and Eckart [21] for the spherical tensor Y_λ presented in (12) and (13), and by considering parity selection rules, the single particle matrix elements of multi-pole operators which are presented in these equations can be rewritten as

$$\langle \mathrm{f} \parallel Q_\lambda \parallel \mathrm{i} \rangle = \frac{e}{\sqrt{4\pi}} (-1)^{j_i+\lambda-\frac{1}{2}} \frac{1+(-1)^{l_\mathrm{i}+l_\mathrm{f}+\lambda}}{2} \cdot \hat{\lambda}\hat{j}_\mathrm{i}\hat{j}_\mathrm{f} \begin{pmatrix} j_\mathrm{f} & j_\mathrm{i} & \lambda \\ \frac{1}{2} & -\frac{1}{2} & 0 \end{pmatrix} R_\mathrm{fi}^{(\lambda)}\,, \tag{15}$$

$$\langle \mathrm{f} \parallel M_\lambda \parallel \mathrm{i} \rangle = \frac{\mu_\mathrm{N}/c}{\sqrt{4\pi}} (-1)^{j_i+\lambda-\frac{1}{2}} \frac{1-(-1)^{l_\mathrm{i}+l_\mathrm{f}+\lambda}}{2} \cdot \hat{\lambda}\hat{j}_\mathrm{i}\hat{j}_\mathrm{f} \begin{pmatrix} j_\mathrm{f} & j_\mathrm{i} & \lambda \\ \frac{1}{2} & -\frac{1}{2} & 0 \end{pmatrix} (\lambda-\kappa) \cdot \left[g_l \left(1 + \frac{\kappa}{\lambda+1} \right) - \frac{1}{2} g_s \right] R_\mathrm{fi}^{(\lambda-1)}\,, \tag{16}$$

which contains the usual abbreviation, the 'hat factors'

$$\hat{\lambda} \equiv \sqrt{2\lambda+1}\,, \quad \hat{j}_{\mathrm{i(f)}} \equiv \sqrt{2j_{\mathrm{i(f)}}+1}\,. \tag{17}$$

μ_N is the nuclear magneton, and $R_\mathrm{fi}^{(\lambda)}$ and κ are defined by the following relations:

$$R_\mathrm{fi}^{(\lambda)} = \int_0^\infty \phi_{n_\mathrm{f} l_\mathrm{f}}(r) r^\lambda \phi_{n_\mathrm{i} l_\mathrm{i}}(r) r^2 \,\mathrm{d}r\,, \tag{18}$$

$$\kappa \equiv (-1)^{l_\mathrm{i}+j_\mathrm{i}+\frac{1}{2}} \left(j_\mathrm{i} + \frac{1}{2} \right) + (-1)^{l_\mathrm{f}+j_\mathrm{f}+\frac{1}{2}} \left(j_\mathrm{f} + \frac{1}{2} \right). \tag{19}$$

Further, $\begin{pmatrix} j_\mathrm{f} & j_\mathrm{i} & \lambda \\ \frac{1}{2} & -\frac{1}{2} & 0 \end{pmatrix}$ is the $3j$ Wigner symbol [22]. $3j$ Wigner symbols are evaluated by the following modified Wigner's formula [23]:

$$\begin{pmatrix} j_1 & j & j_2 \\ m_1 & m & m_2 \end{pmatrix} = \triangle(j_1, j_2, j) \cdot \sqrt{\frac{(j_2-m_2)!(j_2+m_2)!}{(j+m)!(j-m)!(j_1-m-m_2)!(j_1+m+m_2)!}} \times \sum_z (-1)^{2j-j_1-m_1+z} \cdot \frac{(j+j_2-m-m_2-z)!(j_1+m_1+m_2+z)!}{z!(j_2-m_2-z)!(u-z)!(j_2+m_2-u+z)!}\,, \tag{20}$$

where $u = j - j_1 + j_2$ and

$$\triangle(j_1, j_2, j) = \left\{ \left[(j_1+j-j_2)!(j_1-j+j_2)! \cdot (-j_1+j+j_2)! \right] \left[(j_1+j+j_2+1)! \right]^{-1} \right\}^{\frac{1}{2}}. \tag{21}$$

The z value satisfies the following inequality:

$$0 < z \le \min(j_2 - m_2, u)\,. \tag{22}$$

Obviously, the relations $|j_1 - j_2| \le j \le j_1 + j_2$ and $-j \le m \le j$ should also be taken into account.

In order to obtain numerical values of the reduced single-particle matrix elements that are presented by (15) and (16), we need to calculate the radial integrals $R_\mathrm{fi}^{(\lambda)}$ stated in (18). These quantities can be calculated using the radial wave functions $\phi_{nl}(r)$ which were calculated numerically in the previous section. A simple estimate of the reduced transition probabilities, introduced by Weisskopf [24] is the so-called

Table 3. Transition probabilities $T_{\rm fi}^{(\sigma\lambda)}$ $(\sec)^{-1}$ for predominate Eλ and Mλ transitions ($B(\sigma\lambda)$ in $[e^2(\mathrm{fm})^{2\lambda}]$) unit. In the second column, the -1 sign is used for a hole; π and ν are proton and neutron labels, respectively.

Nucleus	Transition mode (i → f)	predominate Eλ	$T_{\rm fi}^{(\sigma\lambda)}$ (W. u.)	$T_{\rm fi}^{(\sigma\lambda)}$ (HO)	$T_{\rm fi}^{(\sigma\lambda)}$ (W–S)
^{15}N	$(\pi^1 p_{3/2})^{-1} \to (\pi^1 p_{1/2})^{-1}$	E2	$3.416\cdot10^{13}$	$5.438\cdot10^{13}$	$2.915\cdot10^{13}$
		M1	$7.477\cdot10^{15}$	$7.439\cdot10^{15}$	$4.995\cdot10^{15}$
^{15}O	$(\nu^1 p_{3/2})^{-1} \to (\nu^1 p_{1/2})^{-1}$	E2	0	0	0
		M1	$4.832\cdot10^{15}$	$4.822\cdot10^{15}$	$3.527\cdot10^{15}$
^{17}O	$\nu^2 s_{1/2} \to \nu^1 d_{5/2}$	E2	0	0	0
		M3	$3.484\cdot10^{6}$	$3.113\cdot10^{6}$	$2.924\cdot10^{6}$
^{17}F	$\pi^2 s_{1/2} \to \pi^1 d_{5/2}$	E2	$2.430\cdot10^{11}$	$2.196\cdot10^{11}$	$2.215\cdot10^{11}$
		M3	$1.596\cdot10^{6}$	$1.442\cdot10^{6}$	$1.455\cdot10^{6}$

Table 4. Allowed electromagnetic multi-pole transition decay half-lives $t_{1/2}$ (sec).

Nucleus	Transition mode (i → f)	$t_{1/2}$ (W. u.)	$t_{1/2}$ (HO)	$t_{1/2}$ (W–S)	$t_{1/2}$ (Exp.)
^{15}N	$(\pi^1 p_{3/2})^{-1} \to (\pi^1 p_{1/2})^{-1}$	$9.270\cdot10^{-17}$	$9.249\cdot10^{-17}$	$1.379\cdot10^{-16}$	$1.5\cdot10^{-16}$ [17]
^{15}O	$(\nu^1 p_{3/2})^{-1} \to (\nu^1 p_{1/2})^{-1}$	$1.432\cdot10^{-16}$	$1.437\cdot10^{-16}$	$1.965\cdot10^{-16}$	–
^{17}O	$\nu^2 s_{1/2} \to \nu^1 d_{5/2}$	$1.989\cdot10^{-7}$	$2.226\cdot10^{-7}$	$2.370\cdot10^{-7}$	–
^{17}F	$\pi^2 s_{1/2} \to \pi^1 d_{5/2}$	$2.852\cdot10^{-12}$	$3.156\cdot10^{-12}$	$3.12\cdot10^{-12}$	–

Table 5. Theoretical and experimental non-zero electromagnetic multi-pole moment for typical one-particle and one-hole mirror nuclei. E2 has the unit of area (barn), and M1 has the unit of the nuclear magneton $\mu_{\rm N}$.

Nuclei	state	$\sigma\lambda$	$M(\sigma\lambda)$ (W. u.)	$M(\sigma\lambda)$ (HO)	$M(\sigma\lambda)$ (W–S)	$M(\sigma\lambda)$ (Exp.)
^{15}N	$(\pi^1 p_{1/2})^{-1}$	M1	-0.264	-0.264	-0.264	-0.28 [25]
	$(\pi^1 p_{3/2})^{-1}$	M1	3.793	3.793	3.793	–
		E2	-0.023	-0.030	-0.029	–
^{15}O	$(\nu^1 p_{1/2})^{-1}$	M1	0.638	0.638	0.638	0.72 [25]
	$(\nu^1 p_{3/2})^{-1}$	M1	-1.913	-1.913	-1.913	–
^{17}O	$(\nu^1 d_{5/2})$	M1	-1.913	-1.913	-1.913	-1.89 [25]
	$(\nu^2 s_{1/2})$	M1	-1.913	-1.913	-1.913	–
^{17}F	$(\pi^1 d_{5/2})$	M1	4.793	4.793	4.793	4.72 [25]
		E2	-0.036	-0.061	-0.074	0.058 [26]
	$(\pi^2 s_{1/2})$	M1	2.79	2.79	2.79	–

Weisskopf unit (W. u.). In this estimation, the radial wave function is assumed to be constant inside the nucleus and zero outside. Using the normalization condition, this simple radial wave function is produced as

$$\phi_{nl}(r) = \begin{cases} \sqrt{\frac{3}{R^3}} & r \le R, \\ 0 & r > R, \end{cases} \tag{23}$$

where R is the nuclear radius.

The γ-decay half-life from an initial state (i) to a final state (f) is

$$t_{1/2} = \frac{\ln 2}{T_{\rm fi}}. \tag{24}$$

The transition probabilities and the γ-decay half-lives for under study mirror nuclei between initial low-lying exited state and final ground state are listed in Tables 3 and 4. The initial and final single particle radial wave functions used to calculate these half-lives are obtained by considering two models of mean-field potentials, using the Weisskopf unit.

The static electric and magnetic multi-pole moments are important observable of nuclear structure. These moments are sensitive to details of the wave function used for computing them. Comparison of computed multi-pole moments with the measured ones is a powerful test to check the validity of a nuclear model. Also, multi-pole coefficients are a measure of typical deformations. The 2^λ-electromagnetic multi-pole moment of a nucleus in a certain state after applying the Wigner–Eckart theorem is obtained by the equation

$$M(\sigma\lambda) = \begin{pmatrix} J & \lambda & J \\ -J & 0 & J \end{pmatrix} \left(\xi, j \,\|\, \begin{pmatrix} Q_\lambda \\ M_\lambda \end{pmatrix} \| \, \xi, j \right), \tag{25}$$

where ξ carries all other quantum numbers. Q_λ and M_λ are the single particle multi-pole tensor operators for electric and magnetic transitions in usual notation with Condon–Shortley phase convention [19]

which are calculated through (12) and (13), respectively. The electric and magnetic multi-pole moments are calculated by using wave functions of the complete set of Woods–Saxon, harmonic oscillator Hamiltonian, and Weisskopf unit estimation; the non-zero values are shown in Table 5. The necessary conditions for a non-vanishing M_1 and E_2 moment are $J \geq \frac{1}{2}$ and $J \geq 1$, respectively. These conditions can already be read from the $3\,j$ symbol in (20). The electric quadrupole moment has the unit of area (barn), and the magnetic dipole moment has the unit of the nuclear magneton μ_N.

4. Conclusion

In this study, electromagnetic moments, electromagnetic multi-pole transition probability, and half-lives of one-particle $^{15}\mathrm{O}-{}^{15}\mathrm{N}$ and one-hole $^{17}\mathrm{O}-{}^{17}\mathrm{F}$ mirror isotopes are calculated numerically. The radial wave functions are computed by considering of two model phenomenological nuclear mean-field potentials: Woods–Saxon and harmonic oscillator potentials. The accessible experimental data confirm the theoretical results of this research. The calculated electromagnetic transition half-life based on the complete set of potential consisting Woods–Saxon potential has a good consistency with the available experimental value of $^{15}\mathrm{N}$.

The theoretical and experimental single-particle magnetic dipole moments of the ground state, shown in Table 5, are agree well with each other. The computed and measured values of the single particle electric quadrupole moment for the $^1d_{5/2}$ state of $^{17}\mathrm{F}$ are also in accordance. The negative computed values of the single particle quadrupole moments confirm the fact that in the defined state with $M = J$, particles move around the nuclear equator and thus produce an oblate shape. In the absence of sufficient laboratory results of electromagnetic multi-pole moments and half-lives for reviewed nuclei, it was not possible to compare the calculated results with experimental ones.

By comparing the available experimental data and the numerically computed values shown in Tables 1 – 5, it may be concluded that the mean-field potential and especially the Woods–Saxon potential can yield dependable results to describe the nuclear structure of nuclei with spherical symmetry.

[1] A. Bohr and B. R. Mottelson, Nuclear Structure, Volume I, W. A. Benjamin, Inc., New York 1969.
[2] M. A. Preston and R. K. Bhaduri, Structure of the Nucleus, Addison-Wesley, New York 1975.
[3] J. Suhonen, From Nucleons to Nucleus, Springer, Berlin, Heidelberg, New York 2007.
[4] L. S. Costa, F. V. Prudenter, P. H. Acioli, J. J. S. Neto, and J. D. M. Vianna, J. Phys. B **32**, 2461 (1999).
[5] S. Cwiok, J. Dudek, W. Nazarewicz, J. Skalski, and T. Werner, Comput. Phys. Commun. **46**, 379 (1987).
[6] M. Brack, Rev. Mod. Phys. **65**, 677 (1993).
[7] Z. Lojewski and J. Dudek, Acta Physics Polonica B **29**, 1 (1998).
[8] J. Sadeghi and M. R. Pahlavani, Afr. J. Math. Phys. **1**, 195 (2004).
[9] M. R. Pahlavani, J. Sadeghi, and M. Ghezelbash, App. Sci. **11**, 106 (2009).
[10] S. M. Ikhdair and R. Sever, Ann. Physik **16**, 218232 (2007).
[11] C. Berkdemir, A. Berkdemir, and R. Sever, Int. J. Mod. Phys. C **20**, 651 (2009).
[12] S. A. Moszkowski, Theory of Multipole Radiation, North-Holland, Amsterdam 1965.
[13] J. Blomquist and S. Wahlborn, Ark. Fiz. **16**, 543 (1960).
[14] J. Blomqvist and A. Molinari, Nucl. Phys. A **106**, 545 (1968).
[15] J. G. F. Francis, Comput. J. **4**, 265 (1961); ibid. 332 (1962).
[16] A. Gilat and V. Subramaniam, Numerical Methods for Engineers and Scientists, John Wiley & Sons, Inc., New York 2008.
[17] R. B. Firestone, V. S. Shirley, S. Y. F. Chu, C. M. Baglin, and J. Zipkin, Table of Iso-topes, Wiley-Interscience, New York 1996; and See website http://ie.lbl.gov/ensdf/.
[18] V. A. Fock, Z. Phys. **61**, 126 (1930).
[19] E. U. Condon and G. H. Shortley, The Theory of Atomic Spectra, Cambridge University Press, Cambridge 1935.
[20] E. P. Wigner, Gruppentheorie, Vieweg, Braunschweig 1931.
[21] C. Eckart, Rev. Mod. Phys. **2**, 305 (1930).
[22] M. Rotenberg, R. Bivins, N. Metropolis, and J. K. Wooten Jr, The 3j and 6j Symbols, M.I.T. Technology Press, Cambridge 1959.
[23] Sh. Tao Lai, Int. J. Quantum Chem. **52**, 593 (1994).
[24] V. F. Weisskopf, Phys. Rev. **83**, 1073 (1951).
[25] http://www.nndc.bnl.gov/nndc/stone_moments/moments.html.
[26] http://www.uni-due.de/physik/wende/englisch/nuclear-moments.pdf.